RSC Advances

ROYAL SOCIETY OF CHEMISTRY

www.rsc.org/advances

Bifunctional application of sodium cobaltate as catalyst and captor through CO oxidation and subsequent CO_2 chemisorption processes

Elizabeth Vera,[1] Brenda Alcántar-Vázquez,[1] Yuhua Duan[2] and Heriberto Pfeiffer[1,*]

[1]*Instituto de Investigaciones en Materiales, Universidad Nacional Autónoma de México, Circuito exterior s/n, Cd. Universitaria, Del. Coyoacán C.P. 04510, México DF, Mexico.*

[2]*National Energy Technology Laboratory, U.S. Department of Energy, Pittsburgh, Pennsylvania 15236, USA.*

**Corresponding author. Phone: +52 (55) 5622 4627, Fax: 52 (55) 5616 1371, Email: pfeiffer@iim.unam.mx*

Abstract

The potential bifunctional mechanism of sodium cobaltate ($NaCoO_2$) in the catalysis of CO oxidation and subsequent CO_2 chemisorption was systematically analysed. Different catalytic and gravimetric experiments were performed dynamically and isothermally at multiple temperatures. Initially, the CO oxidation process was evaluated using a catalytic reactor connected to a gas chromatograph. Once the production of CO_2 was confirmed, its chemisorption capacity with $NaCoO_2$ was studied gravimetrically. Catalytic and gravimetric analysis products were studied by XRD, FTIR and SEM to elucidate the double reaction mechanism. Sodium cobaltate exhibited interesting catalytic properties over a wide temperature range, although the $NaCoO_2$ crystalline structure and chemical composition changed during the CO_2 capture process. Furthermore, all the experiments were

theoretically supported by first-principles density functional theory thermodynamic calculations. The calculated thermodynamic properties of the CO oxidation and CO_2 capture reactions with $NaCoO_2$ under different oxidation conditions were in good agreement with the experimental measurements.

Keywords; CO oxidation; CO_2 chemisorption; sodium cobaltate, ab initio thermodynamics calculations

Introduction

Humanity would not be able to survive in the modern era without utilizing large amounts of energy, and fossil fuels have become essential for providing this energy. However, the use of carbonaceous fuels has resulted in huge amounts of CO_2 emissions, which brings with it a slew of known environmental implications. Thus, one of the most important scientific challenges today concerns the development of alternatives for satisfying energy demands while protecting the environment.

Within this context, over the last several years, important research progress has been made in the development of solid CO_2 capture materials. Based on the CO_2 capture temperature, these materials can be divided in three main groups: i) low temperature captors (T < 200 ºC), ii) moderate temperature sorbents (200-400 ºC) and iii) high temperature captors (T > 400 ºC) [1-3]. Among the high temperature captors studied are various alkaline ceramic materials [4-5]. Some of these binary-metal oxides, containing at least one alkaline element, have been considered potential CO_2 captors, as their chemical basicity renders them able to chemisorb CO_2. Since 1998, the most studied ceramics have

included lithium silicates (Li_4SiO_4 and Li_8SiO_6), pentalithium aluminate (Li_5AlO_4), lithium zirconates (Li_2ZrO_3, $Li_6Zr_2O_7$, and Li_8ZrO_6), lithium cuprate (Li_2CuO_2) and sodium zirconate (Na_2ZrO_3), as well as others [4-19].

However, as previously mentioned, equally important to CO_2 capture are improvements in energy efficiency, conversion processes and alternative energy sources. In this sense, there are several studies where hydrogen is produced as an alternative energy vector using materials that are similar to those previously mentioned for the CO_2 capture process [20-27]. Some of these mechanisms correspond to different reforming reactions [21-23, 25-26] and biomass reactions [24]. Of course, most of these reactions produce synthetic gas, also known as syngas, which ideally is composed of H_2 and CO or CO_2. Therefore, hydrogen enrichment depends on the successful separation of H_2 from the carbon oxides present. Here, alkaline thermal treatment has been proposed as a novel process for H_2 enrichment using biomass under moderate thermal conditions [28-29]. Additionally, in steam reforming (SR), the H_2/CO ratio can be varied by manipulating the relative concentrations of CO_2 and O_2 in the feed, which in turn can be achieved by selectively adsorbing the co-generated CO_2 on an appropriate sorbent and/or by carbon monoxide oxidation [30]. Noble metal catalysts, especially gold-based catalysts, have shown high activity for CO oxidation [31-32]. However, due to the high prices and scarcity of noble metals, the less costly transition metal oxides have been considered promising catalysts for eliminating the CO from reformed fuels [33-37]. Among them, cobalt oxide catalysts have been extensively studied. Depending on the synthesis method and the reaction conditions employed, Co_3O_4 shows different activity in CO oxidation and oxygen evolution [33, 36-37].

Additionally, it has been reported recently that Na_2ZrO_3 and $NaCoO_2$ seem to have the capacity to act as bifunctional materials, acting as a catalyst during CO oxidation and subsequently as a CO_2 chemisorbent [38-39]. As such, all these materials and processes may be of great interest for use in next-generation H_2 purification technologies. Unfortunately, due to the complexity of the reactions and systems involved, they are poorly understood. The aim of this work was to analyse the bifunctional ability of sodium cobaltate for use as a CO oxidation catalyst and as a CO_2 chemisorbent. Both processes were evaluated dynamically and isothermally at different temperatures, varying the gas mixtures, to determine the catalytic and chemisorption reaction processes, as well as to determine the rate limiting step of the whole process. Additionally, the experiments were theoretically supported by first-principles density functional theory (DFT) thermodynamic calculations.

Experimental and computational methods

Sodium cobaltate ($NaCoO_2$) was synthesized by a solid-state reaction, and its composition and microstructure have been previously reported [38]. Elemental analysis showed that the real chemical composition of the sample was equal to $Na_{0.89}CoO_{1.95}$, although the sample is labelled as $NaCoO_2$ here.

The CO oxidation reaction was carried out and analysed in a Bel-Rea catalytic reactor (Bel Japan), using $NaCoO_2$ (200 mg) and a gas mixture of 5 vol% O_2 (Praxair, grade 2.6), 5 vol% CO and N_2 (Praxair, certificate mixture) as balance with a total flow rate of 100 mL/min. For the dynamic analysis, the sample was heated from 30 to 900 ºC at a

heath rate of 5 ºC/min. Then, the $NaCoO_2$ sample was isothermally analysed in the same flux at different temperatures (from 300 to 700 ºC). Prior to all the analyses, the sample was cleaned under a 50 mL/min N_2 (Praxair, grade 4.8) flow for 15 minutes. The samples were heated to the desired temperature under a N_2 flow. Once the corresponding temperature was reached, the flow gas was switched from N_2 to the mixture mentioned above. The gas products were analysed in a GC 2014 gas chromatograph (Shimadzu) with a Carboxen-1000 column and with an Alpha Platinum FTIR (Bruker) connected to a ZnS gas flow cell.

To analyse the *in-situ* chemisorption of the CO_2 generated by the CO oxidation reaction, different dynamic and isothermal experiments were performed on a Q500HR thermobalance (TA Instruments). Initially, the sample was dynamically heated from 30 to 850 ºC at a heath rate of 5 ºC/min using 60 mL/min of CO_2, CO or CO-O_2 (all diluted in N_2). Then, the $NaCoO_2$ sample was isothermally analysed in the same gas flow at different temperatures (from 300 to 700 ºC). For the isothermal analysis, the samples were heated to the desired temperature under a N_2 flow (Praxair, grade 4.8). Once the corresponding temperature was reached, the flow gas was switched from N_2 to the gas mixture.

The structural and microstructural evolution of the products after CO oxidation and subsequent CO_2 chemisorption analysis were studied by XRD using a diffractometer (Siemens, D5000) with a Co-Kα radiation at 34 kV and 30 mA. The phases were identified using the Joint Committee Powder Diffraction Standards (JCPDS). Additionally, the products were analysed by FTIR using Alpha Platinum equipment from Bruker connected to a diamond attenuated total reflectance (ATR) cell. The microstructural evolution was analysed in a JEOL JMS-7600F scanning electron microscope.

To better understand the experimental results, different theoretical calculations on the thermodynamic properties of the relevant reactions were performed. Because the thermodynamic properties of the capture reactions between $NaCoO_2$ and CO_2 or CO and O_2 are not available in the literature, the *ab initio* thermodynamic calculations were performed on the following reactions by combining density functional theory (DFT) with lattice phonon dynamics. More detailed descriptions of the calculation method can be found in previous studies [40-41]. The mechanism by which $NaCoO_2$ captures CO_2 or CO can be expressed with the following three reactions (for convenience, the reaction was normalized to 1 mole of CO_2 or CO):

$$2\ NaCoO_2 + CO_2 \rightarrow Na_2CO_3 + Co_2O_3 \qquad (1)$$

$$2\ NaCoO_2 + CO \rightarrow Na_2CO_3 + 2\ CoO \qquad (2)$$

$$2\ NaCoO_2 + CO + {}^1/_2\ O_2 \rightarrow Na_2CO_3 + Co_2O_3 \qquad (3)$$

In the above reactions, CO_2, CO and O_2 were treated as ideal gases. Therefore, the difference between the Gibbs free energy (ΔG^o) of the solid phases of reactants and products may be approximated by the difference in their total energies (ΔE_{DFT}), obtained directly from DFT calculations and the vibrational free energy of the phonons. Ignoring the PV contribution terms for solids, the variation of the Gibbs free energy (ΔG) for these reactions as a function of temperature and pressure can be written as:

$$\Delta G\ (T, P) = \Delta G^0(T) - RT\ \ln(P_{gas}/P_o) \qquad (4)$$

where

$$\Delta G^0(T) \approx \Delta E_{DFT} + \Delta E_{ZP} + \Delta F_{PH}\ (T) - G^0_{gas}\ (T) \qquad (5)$$

ΔE_{DFT} is the DFT energy difference between the reactants and products of the capture reactions (1 to 3); ΔE_{ZP} is the zero point energy difference between the reactants and products and can be obtained directly from phonon calculations; and ΔF_{PH} is the phonon free energy change excluding zero-point energy (which is already counted into the ΔE_{ZP} term) between the reactants and products solids phases. P_{gas} is the partial pressure of CO_2 or CO in the gas phase (in reaction 3, CO and O_2 are involved, so $P_{gas} = P_{CO} \times P_{O_2}^{0.5}$) and P_0 is the standard state reference pressure, taken to be 1 bar. The heat of reaction ($\Delta H^{cal}(T)$) can be evaluated through the following equation:

$$\Delta H^{cal}(T) = \Delta G^{0}(T) + T(\Delta S_{PH}(T) - S_{gas}(T)) \qquad (6)$$

where $\Delta S_{PH}(T)$ is the difference in entropies between the solid products and reactants. The CO_2, CO and O_2 free energies (G^{0}_{gas}) can be obtained by way of standard statistical mechanics [41-42], while their entropies (S_{gas}) can be found in empirical thermodynamic databases [43]. The DFT calculations with plane-wave basis sets and pseudopotential approximations were performed to describe the structural, energetic and electronic properties of the solids considered in this study. All calculations were performed using the Vienna *ab initio* simulation package (VASP) [44-45]. In this study, the PAW pseudo-potentials and PW91 exchange-correlation functional were used in all of the calculations [46]. Plane wave basis sets were used with a kinetic energy cutoff of 520 eV and an augmentation charge cutoff of 605.4 eV. The k-point sampling grids of $m \times n \times l$, obtained using the Monkhorst-Pack method [47], are used for these bulk calculations, where m, n, and l are determined with a spacing of approximately 0.028 $Å^{-1}$ along the reciprocal axes of their unit cells. In the phonon calculations, for each generated supercell, displacements of 0.03 Å of non-equivalent atoms were generated. The solids with hexagonal structures were

built in orthorhombic supercells with the option of restoring the symmetry of the crystal space group. Then, for each supercell, the DFT calculations were performed again to obtain the force on each atom due to the displacements. These forces were carried back to PHONON package [48] to calculate the phonon dispersions and densities from which the partition function could be applied and used to obtain free energies and entropies as shown in Eqs. (4)-(6).

Results and discussion

The most stable crystal structures of $NaCoO_2$, Co_2O_3 and CoO are shown in Figure 1, and their corresponding space groups are $R\bar{3}m$ (No. 166), $R\bar{3}cH$ (No. 167), and $Fm\bar{3}m$ (No. 225), respectively [49-51]. Table 1 summarizes the optimized structure parameters and calculated energetic properties of each crystal structure, which are further used for evaluating the capture reactions as described in the following sections.

Initially, the CO conversion to CO_2 was evaluated dynamically and isothermally in a catalytic reactor; as expected, the degree of CO conversion increases as a function of temperature and mass/flow ratio. In fact, the point of 100 % efficiency of CO conversion was shifted from 570 to 490 and 450 ºC, using 50, 200 and 250 mg, respectively (data not shown). When using 200 mg of $NaCoO_2$, the CO conversion to CO_2 was evidenced beginning at 115 ºC, and total conversion was obtained between 450 and 900 ºC. However, the CO_2 and O_2 concentrations varied between 740 – 900 ºC and 820 – 900 ºC, respectively. Both concentrations tended to increase, although CO conversion was complete. At the highest temperatures, the increase in CO_2 concentration may be associated with $NaCoO_2$

decarbonation, which occurs in this temperature range. Therefore, the CO_2 quantified corresponds to the amount of CO catalytically converted at that specific temperature as well as to the fraction of the produced CO_2 that was previously chemisorbed on the $NaCoO_2$. On the other hand, the increase in oxygen concentration must be associated with the cobalt oxide reduction process. According to previous investigations, the Co_2O_3 produced during carbonation can be reduced to Co_3O_4 and consecutively to CoO, releasing oxygen [38].

The results show that using higher amounts of sodium cobaltate did not reduce the CO conversion temperature significantly. Therefore, all subsequent experiments were performed using 200 mg of $NaCoO_2$ and the same CO-O_2 mixture and flow rate. Different isothermal experiments were performed, and the products obtained were re-characterized by XRD and ATR-FTIR to confirm the CO oxidation and the consecutive CO_2 chemisorption. Figure 2 shows the CO conversion isotherms obtained at different temperatures. The initial isothermal experiment was performed at 300 °C. This isotherm exhibited decreasing exponential behaviour, in which equilibrium was not reached after 5 hours, and the conversion efficiency decreased from 46 to 25%. As previously described, $NaCoO_2$ is able to convert CO to CO_2, but it is also able to trap CO_2 chemically. Thus, $NaCoO_2$ carbonation may partially inhibit CO conversion due to the formation of a Na_2CO_3-Co_3O_4 external shell (as discussed below). When the isotherms were performed between 350 and 450 ºC, the same tendency to decrease was observed, although the CO conversion increased. In fact, at 450 ºC, the CO conversion efficiency was approximately 75 %. Finally, at higher temperatures (500-700 ºC), CO was completely converted throughout the whole isothermal experiment.

All the isothermal products were analysed by XRD and ATR-FTIR, as is shown in Figure 3, to probe the $NaCoO_2$ carbonation process. The XRD patterns of the products mainly showed the formation of Co_3O_4, the rate of which increased with increasing temperature, while the amount of $NaCoO_2$ decreased. The formation of this cobalt oxide may be associated with the CO_2 carbonation process. Nevertheless, Na_2CO_3 formation was not totally proven by this technique, it may be due to the difference in cobalt and sodium diffraction scatter factors. Thus, ATR-FTIR spectra of these samples were obtained, and the results of this spectroscopic analysis confirmed the formation of carbonate species (CO_3^{2-}), which must correspond to the presence of Na_2CO_3. Therefore, although CO is catalytically converted to CO_2, part of it must be chemically trapped to produce Na_2CO_3 and Co_3O_4 until the sodium cobaltate is saturated [38].

The catalytic activity was evaluated over 24 hours (data not shown) at 650 ºC. The isotherm curve obtained showed a small degree of deactivation of 3.5 ± 1 % during the first three hours, but, after five hours, the reaction tended to stabilize at ~99 % CO conversion, which suggests a good thermal stability of the $NaCoO_2$ as a catalyst for the CO oxidation process. This result strongly suggests that initially CO is oxidized by $NaCoO_2$ and latter it is continued by the different cobalt oxides produced after the carbonation process.

The calculated thermodynamic properties of $NaCoO_2$ capturing CO_2 or CO are shown in Figure 4. As can be observed, the mechanisms of CO_2 or CO capture by $NaCoO_2$ possess Gibbs free energy differences that are not excessively large. This is an interesting result considering that, in the CO reaction, more oxygen atoms have to be taken from the $NaCoO_2$ structure. However, if O_2 is introduced into the CO capture reaction, it causes a huge variation in the thermodynamic properties of the reaction. This can be explained by the fact that the CO-O_2 oxidation reaction produces large amounts of heat. Figure 5 shows

the calculated vant Hoff Plots of the relationships among the free energy (ΔG), temperature (T) and gas pressure (P in logarithmic scale). In this figure, only ΔG = 0 curves are shown. Table II summarizes the calculated thermodynamic properties of these reactions and the corresponding turnover T. From Figure 5 and Table II, it can be observed that $NaCoO_2$ would capture CO_2 or CO (especially if O_2 is introduced) up to a very high temperature, but it has to be taken into account that Na_2CO_3 decomposes at 852 ºC. For example, when the P_{CO_2}=0.1 bar, corresponding to the post-combustion condition, the turnover T is approximately 450 ºC. Above this temperature, $NaCoO_2$ does not capture any additional CO_2, and it starts to release CO_2.

To further analyse and evidence the *in-situ* production and chemisorption of CO_2, different thermogravimetric analyses were performed. Figure 6-A shows the dynamic thermograms of $NaCoO_2$ using three different gases: CO_2, CO and CO-O_2, all of which were diluted in N_2, with a P_{CO} or P_{CO_2} of 0.05. When the $NaCoO_2$ sample was thermally heated in flowing CO_2, it exhibited a small weight decrease (~2 wt%) between 30 and 85 ºC, which was associated with a superficial dehydration process. Then, between 120 and 420 °C, the sample presented practically no superficial CO_2 chemisorption, a behaviour typically observed in alkaline ceramics. This observation must also be related to the P_{CO_2} value of 0.05 used, which modifies the sorption-desorption dynamic equilibrium. On the other hand, the bulk CO_2 chemisorption was observed between 450 and 745 ºC. After the weight increase, a weight loss due to the sample decarbonation and decomposition processes was observed. Likewise, it had been already shown that a $NaCoO_2$-CO-O_2 system [39] presented a similar trend to that observed with CO_2, confirming the occurrence of CO oxidation and subsequent CO_2 chemisorption. In this case, the superficial and bulk chemisorption processes were observed between 280 and 440 ºC and between 440 and 805

ºC, respectively. It must be noted that both processes are shifted to higher temperatures in comparison with the CO_2 case, which may be related to a different reaction mechanism because, in this case, a double process is taking place (that is, both CO oxidation and the subsequent CO_2 chemisorption are taking place).

Conversely, the $NaCoO_2$ dynamic thermogram obtained merely with CO and in the absence of O_2 showed a different behaviour. The $NaCoO_2$-CO thermogram did not show any significant increase in weight, as in the previous cases. This thermogram initially showed a weight decrease related to dehydration (≤100 ºC) and dehydroxylation (350-400 ºC) processes. Then, between 500 and 630 ºC, the thermogram showed a slight weight increase of approximately 0.5 wt%. In the same temperature range, the $NaCoO_2$-CO_2 and $NaCoO_2$-CO-O_2 systems chemisorbed CO_2, which suggests that $NaCoO_2$ is partially trapping CO_2. Figure 6-B supports these results, showing the catalytic dynamic evolutions of CO consumption and CO_2 formation in comparison to the thermogravimetric analysis and using $NaCoO_2$ in the absence of oxygen. Between room temperature and 430 ºC, the CO concentration did not vary, and CO_2 was not detected, indicating negligible CO conversion. From this temperature to 630 ºC, the presence of CO_2 was observed, which is in agreement with the decrease in CO present. Thus, CO is being partially converted to CO_2 even in the absence of oxygen, which must be released from the $NaCoO_2$ structure. This behaviour has been reported for other transition metal oxides where the CO adsorbed on the metal sites is oxidised by the lattice oxygen atoms [33, 53-54]. This result is also in accord with the thermogravimetric curve, which shows a partial increase in weight. Therefore, the degree of catalytic oxidation of CO and the subsequent chemisorption of CO_2 by $NaCoO_2$ is significantly reduced in the absence of oxygen. It can be assumed from this that the CO

oxidation process is a conditioning step for the CO oxidation and CO_2 chemisorption bifunctionality.

Different isothermal experiments were performed to further analyse the chemisorption functionality of $NaCoO_2$. Figure 7 shows the $NaCoO_2$ isotherms obtained at different temperatures in a CO-O_2 flux. The initial isothermal experiment was performed at 300 °C and exhibited an exponential behaviour, failing to reach equilibrium after 3 hours and exhibiting a weight increase of only 1.9 wt%. Subsequent isotherms were performed between 400 and 700 ºC. All of these isotherms exhibited a similar exponential behaviour where the weight increased as a function of temperature from 4.8 wt% at 400 ºC to a maximum of 9.8 wt% at 700 ºC. Expressed another way, the CO_2 capture efficiency increased from 10.7 to 55.4% by increasing the temperature from 300 to 700 ºC. It is important to note here that the catalytic results indicate CO is totally oxidized at $T \geq 500$ ºC.

When the $NaCoO_2$-CO-O_2 isotherms are compared with the $NaCoO_2$-CO_2 isotherms [38], some interesting features are noted (Figure 8). At short times, CO_2 chemisorption is faster in the $NaCoO_2$-CO_2 system than in the $NaCoO_2$-CO-O_2 system. However, at $T \leq 600$ ºC, the final weight increase of the $NaCoO_2$-CO-O_2 system is higher than that of the $NaCoO_2$-CO_2 system. The behaviour presented at short times may be related to a gas concentration effect because the rate of CO_2 production by CO oxidation is as high as 3 mL/min and solid-gas interactions are favoured in the $NaCoO_2$-CO_2 system, resulting in a higher weight increase. On the other hand, the final weight gains may be explained as follows: for $T \leq 400$ ºC, the carbonate shell is formed faster in the $NaCoO_2$-CO_2 system, partially inhibiting the chemisorption process on $NaCoO_2$. At $T \geq 600$ ºC, however, the

chemisorption process in both systems is mainly dependent on intercrystalline diffusion processes. Hence, the final weight gain is similar for the isotherms of both systems.

To analyse the microstructural evolution of $NaCoO_2$, SEM images of the material were obtained (Figure 9). The pristine sample analysed was comprised of polyhedral flake-like particles, as described previously [38]. The CO oxidation products, obtained at 400 and 700 ºC, possessed the same flake-like microstructure, with particle sizes ranging between 1 and 6 μm. For the 400 ºC products, the particles formed non-dense agglomerates, and, in the case of 700 ºC, the agglomerates were slightly denser than in the pristine sample and were approximately 20-60 μm in size. Additionally, the backscattered electron images of both products showed the presence of two different phases, which correspond to Na_2CO_3 (dark phase) and Co_3O_4 (light phase), as previously identified by XRD. At 400 ºC, the Na_2CO_3 and Co_3O_4 phases seem to be homogeneously mixed, whereas, in the sample treated at 700 ºC, these phases tended to segregate. This segregation may enhance the ability of the CO oxidation process to continue in the cobalt oxide phase even when the carbonation process is completed.

Summarizing, $NaCoO_2$ is able to be used into a bifunctional application; where $NaCoO_2$ acts as catalyst and captor through CO oxidation and subsequent CO_2 chemisorption processes. This bifunctional mechanism is represented in the following reaction system:

$$CO + ½\ O_2 \xrightarrow{NaCoO_2} CO_2 + 2\ NaCoO_2 \longrightarrow Na_2CO_3 + Co_2O_3 \qquad (7)$$

where the cobalt oxide composition changes as a function of temperature, varying the cobalt oxidation state and consequently producing oxygen.

Conclusions

Sodium cobaltate was analysed as a possible bifunctional material for CO oxidation and subsequent chemisorption of the CO_2 produced. Initially, catalytic CO oxidation to CO_2 was analysed using gas chromatography in-line with the reactor. The results obtained confirmed that CO can be oxidized by $NaCoO_2$ at different temperatures depending on the mass/flow ratio. On the other hand, the *in-situ* production and chemisorption of CO_2 was analysed using thermogravimetric analysis and was found to follow a similar reaction mechanism to those already reported for alkaline ceramics.

The catalytic and gravimetric results, as well as analysis of the $NaCoO_2$ products, indicated that $NaCoO_2$ is able to catalyse CO to CO_2 and subsequently chemisorb the latter. Of course, the chemisorption of CO_2 changed the $NaCoO_2$ crystalline structure and its composition, transforming it to Na_2CO_3 and different cobalt oxides. Nevertheless, the catalytic effect was not reduced within a certain temperature range, even when an experimental catalytic evaluation was performed during 24 hours. Therefore, CO oxidation occurs on $NaCoO_2$ initially, but, once Na_2CO_3 is produced, the catalytic reaction must be performed on the cobalt oxides, and it is not limited by the Na_2CO_3 formation.

Finally, all of these results were corroborated with theoretical thermodynamic data calculated for the $NaCoO_2$-CO and $NaCoO_2$-CO_2 reaction systems, for which different oxidation conditions were modelled. The ΔH and ΔG values clearly showed the different thermal stabilities for each reaction process depending on temperature. Although CO_2 and CO capture by $NaCoO_2$ have similar ΔH and ΔG values, in the CO reaction, interestingly, more oxygen atoms have to be taken from the $NaCoO_2$ structure. However, when O_2 was

added into the CO capture reaction, the ΔH and ΔG thermodynamic values changed significantly. In fact, the CO-O_2 oxidation reaction produces large amounts of heat, which may explain the ΔH and ΔG variations.

Acknowledgements

This work was financially supported by the projects SENER-CONACYT and PAPIIT-UNAM. E. Vera thanks to CONACYT for financial support. The authors thank to O. Novelo, J. Romero and A. Tejeda for technical help.

References

[1] S. D. Kenarsari, D. Yang, G. Jiang, S. Zhang, J. Wang, A. G. Russell, Q. Wei and M. Fan, *RSC Adv.*, 2013, **3**, 22739-22773.

[2] X. Lu, D. Jin, S. Wei, Z. Wang, C. An and W. Guo, *J. Mater. Chem. A*, 2015, **3**, 12118-12132.

[3] J. Wang, L. Huang, R. Yang, Z. Zhang, J. Wu, Y. Gao, Q. Wang, D. O'Hare and Z. Zhong, *Ener. Environ. Sci.*, 2014, **7**, 3478-3518.

[4] L. K. G. Bhatta, S. Subramanyam, M. D. Chengala, S. Olivera and K. Venkatesh, *J. Clean. Prod.*, 2015, **103**, 171-196.

[5] S. Kumar and S. K. Saxena, *Mater. Renew. Sustain. Ener.*, 2014, **3**, 1-15.

[6] M. B. I. Chowdhury, M. R. Quddus and H. I. deLasa, *Chem. Eng. J.*, 2013, **232**, 139-148.

[7] J. Ortiz-Landeros, T. L. Ávalos-Rendón, C. Gómez-Yáñez and H. Pfeiffer, *J. Therm. Anal. Calorim.*, 2012, **108**, 647-655.

[8] M. R. Quddus, M. B. I. Chowdhury and H. I. deLasa, *Chem. Eng. J.*, 2015, **15**, 347-356.

[9] S. Wang, C. An and Q. H. Zhang, *J. Mater. Chem. A*, 2013, **1**, 3540-3550.

[10] S. Y. Shan, Q. M. Jia, L.H. Jiang, Q. C. Li, Y. M. Wang and J. H. Peng, *Ceram. Int.*, 2013, **39**, 5437-5441.

[11] Z. Qi, H. Daying, L. Yang, Y. Qian and Z. Zibin, *AIChE J.*, 2013, **59**, 901-911.

[12] K. Wang, P. Zhao, X. Guo, Y. Li, D. Han and Y. Chao, *Ener. Convers. Manag.*, 2014, **81**, 447-454.

[13] K. Oh-ishi, Y. Matsukura, T. Okumura, Y. Matsunaga and R. Kobayashi, *J. Solid State Chem.*, 2014, **211**, 162-169.

[14] S. M. Amorim, M. D. Domenico, T. L. P. Dantas, H. J. José and R. F. P. M. Moreira, *Chem. Eng. J.*, 2016, **283**, 388-396.

[15] L. Martinez-dlCruz and H. Pfeiffer, *J. Phys. Chem. C*, 2012, **116**, 9675-9680.

[16] H. A. Lara-García, B. C. Alcántar-Vázquez, Y. Duan and H. Pfeiffer, *RSC Ads.*, 2015, **5**, 34157-34165.

[17] C. Wang, B. Dou, Y. Song, H. Chen, Y. Xu and B. Xie, *Ind. Eng. Chem. Res.*, 2014, **53**, 12744-12752.

[18] A. Sanna, I. Ramli and M. M. Maroto-Valer, *Ener. Procedia*, 2014, **63**, 739-744.

[19] F. Fujishiro, Y. Kojima and T. Hashimoto*, J. Am. Ceram. Soc.*, 2012, **95**, 3634-3637.

[20] R. Raskar, V. Rane and A. Gaikwad, *Water Air Soil Pollut.*, 2013, **224**, 1569-1584.

[21] D. Y. Aceves-Olivas, M. R. Baray-Guerrero, M. A. Escobedo-Bretado, M. M. Silva-Paula, J. Salinas-Gutiérrez, V. Guzmán-Velderrain, A. López Ortiz and V. Collins-Martínez, *Inter. J. Hydrogen Ener.*, 2014, **39**, 16595-16607.

[22] M. H. Halabi, M. H. J. M. de Croon, J. van der Schaaf, P. D. Cobden and J. C. Schouten, *Chem. Eng. J.*, 2011, **168**, 872-882.

[23] M. H. Halabi, M. H. J. M. de Croon, J. van der Schaaf, P. D. Cobden and J. C. Schouten, *Chem. Eng. J.*, 2011, **168**, 883-888.

[24] K. Wang, P. Zhao, X. Guo, D. Han and Y. Chao, *Environ. Prog. Sustain. Ener.*, 2015, **34**, 526-532.

[25] H. K. Rusten, E. Ochoa-Fernández, H. Lindborg, D. Chen and H. A. Jakobsen, *Ind. Eng. Chem. Res.*, 2007, **46**, 8729-8737.

[26] E. Ochoa-Fernández, H. K. Rusten, H. A. Jakobsen, M. Rønning, A. Holmen and D. Chen, *Catal. Today*, 2005, **106**, 41-46.

[27] B. Tsuchiya, K. Morita and S. Nagata, *Surf. Interface Anal.*, 2012, **44**, 717-720.

[28] M. R. Stonor, T. E. Ferguson, J. G. Chen and A.-H. A. Park, *Ener. Environ. Sci.*, 2015, **8**, 1702-1706.

[29] S. N. Reddy, S. Nanda, A. K. Dalai and J. A. Kozinski, *Inter. J. Hydrogen Ener.*, 2014, **39**, 6912-6926.

[30] Z. Guo B. Liu, Q. Zhang, W. Deng, Y. Wang and Y. Yang, *Chem. Soc. Rev.*, 2014, **43**, 3480-3524.

[31] A. Sandoval, C. Louis and R. Zanella, *Appl. Catal. B*, 2013, **140-141**, 363-377.

[32] P. Rodriguez, D. Plana, D. J. Fermin and M. T.M. Koper, *J. Catal.*, 2014, **311**, 182-189.

[33] X. Xie, Y. Li, Z. Q. Liu, M. Haruta and W. Shen, *Nature*, 2009, **458**, 746-749.

[34] M. Y. Guo, F. Liu, J. Tsui, A. A. Voskanyan, A. M. C. Ng, W. K. Chan, K. Y. Chan, C. Liao, K. Shih and C. Surya, *J. Mater. Chem. A*, 2015, **3**, 3627-3632.

[35] J. Q. Lu, C. X. Sun, N. Li, A. P. Jia and M. F. Luo, Appl. Surf. Sci., 2013, **287**, 124-134.

[36] B. Han, D. Qian, M. Risch, H. Chen, M. Chi, Y. S. Meng and Y. Shao-Horn, *J. Phys. Chem. Lett.*, 2015, **6**, 1357-1362.

[37] M. Zhou, L. Cai, M. Bajdich, M. García-Melchor, H. Li, J. He, J. Wilcox, W. Wu, A. Vojvodic and X. Zheng, *ACS Catal.*, 2015, **5**, 4485-4491.

[38] E. Vera, B. Alcántar-Vazquez and H. Pfeiffer, *Chem. Eng. J.*, 2015, **271**, 106-113.

[39] B. Alcántar-Vazquez, E. Vera, F. Buitrón-Cabrera, H. A. Lara-García and H. Pfeiffer, Chem. Lett., 2015, **44**, 480-482.

[40] Y. Duan, H. Pfeiffer, B. Y. Li, I. C. Romero-Ibarra, D. C. Sorescu, D. R. Luebke and J. W. Halley, *Phys. Chem. Chem. Phys.*, 2013, **15**, 13538-13558.

[41] Y. Duan and D. C. Sorescu, *J. Chem. Phys.*, 2010, **133**, 074508.

[42] B. Zhang, Y. Duan and J. K. Johnson, *J. Chem. Phys.*, 2012, **136**, 064516.

[43] M. W. J. Chase, NIST-JANAF Themochemical Tables, 4th edition, *J. Phys. Chem. Ref. Data*, Monograph, 4th edn, 1998, **9**, 1.

[44] G. Kresse and J. Hafner, *Phys. Rev. B*, 1993, **47**, 558-561.

[45] G. Kresse and J. Furthmuller, *Comp. Mater. Sci.*, 1996, **6**, 15-50.

[46] J. P. Perdew and Y. Wang, *Phys. Rev. B*, 1992, **45**, 13244-13249.

[47] H. J. Monkhorst and J. D. Pack, *Phys. Rev. B*, 1976, **13**, 5188-5192.

[48] K. Parlinski, Software PHONON, *Computing for Materials*, Krakow, Poland, 2006.

[49] J. Chenavas, J. C. Joubert and M. Marezio, *Solid State Comm.*, 1971, **9**, 1057-1060.

[50] J. F. Liu, S. Yin, H. P. Wu, Y. W. Zeng, X. R. Hu, Y. W. Wang, G. L. Lv and J. Z. Jiang, *J. Phys. Chem. B*, 2006, **110**, 21588-21592.

[51] Y. Takahashi, Y. Gotoh and J. Akimoto, *J. Solid State Chem.*, 2003, **172**, 22-26.

[52] *HSC Chemistry*, version 6.1, Outotec Research Oy: Pori, Finland, 2006, www.outotec.com/hsc.

[53] F. Mariño, C. Descorme and D. Duprez, *Appl. Catal. B*, 2005, **58**, 175-183.

[54] P. Mars and D. Van Krevelen, *Chem. Eng. Sci.*, 1954, **3**, 41-59.

FIGURE CAPTIONS

Figure 1. $NaCoO_2$ (A), Co_2O_3 (B) and CoO (C) crystal structures of solids involved in this study. Red balls stands for O, purple for Na, blue for Co, and *c* axis is vertical.

Figure 2. CO conversion isothermal analyses using 200 mg of catalysts at different temperatures.

Figure 3. XRD patterns (A) and ATR-FTIR spectra (B) of different CO oxidation isothermal products.

Figure 4. The calculated thermodynamic properties of reactions of $NaCoO_2$ capturing CO_2 or CO *versus* temperature: Heat of reaction (A) and free energy change (B).

Figure 5. Calculated vant Hoff plots of the relationships among the free energy (ΔG), temperature (T) and gas pressure (P in logarithmic scale). Only $\Delta G=0$ curves are shown explicitly.

Figure 6. Dynamic thermograms of $NaCoO_2$ in CO_2 (5 vol% diluted in N_2), CO (5 vol% diluted in N_2) and CO-O_2 (5 and 5 vol% diluted in N_2) flows (A) and CO-$NaCoO_2$ gas evolution into the catalytic reactor (B).

Figure 7. CO-O_2 thermogravimetric isothermal analyses of $NaCoO_2$ at different temperatures.

Figure 8. Isotherms comparison of the $NaCoO_2$-CO-O_2 (blue) and $NaCoO_2$-CO_2 (black) systems at different temperatures (A), and inset of the same isothermal curves at the first times (B). The $NaCoO_2$-CO_2 isotherms were taken from [38].

Figure 9. Scanning electron images of the $NaCoO_2$ pristine sample (A) and the isothermal CO oxidation products at 400 (B) and 700 °C (C).

Table 1. Comparison of the experimental and the DFT structural parameters and energies for the compounds in the reactions studied. The zero-point energy and entropy calculated from phonon density of states, as well as the available experimental data are also listed.

Compound	Space group	Structural parameters		Calculated Energy (eV/f.u.)		Entropy (J/mol.K)	
		experimental	Calculated	E^{DFT}	E_{ZP}	Phonon (T=300K)	Exp.[a] (T=298.15K)
$NaCoO_2$	$R\bar{3}mH$ (No.166) Z=3	a=2.8897 Å c=15.609 Å	a= 2.930265 b= 15.50044	-23.62017	0.27544	63.53	
CoO	$Fm\bar{3}m$(No.225) Z=4	a=4.273 Å	a=4.232817	-12.97780	0.06990	60.25	52.85
Co_2O_3	$R\bar{3}cH$(No.167) Z=6	a=4.782Å c=12.96 Å	a=4.806947 c=13.03805	-34.19846	0.40625	64.72	
Na_2CO_3 [b]	C12/m1(No.12)	a=9.01029 b=5.23116 c=6.34548 β=96.062°	a=8.95180 b=5.33507 c=6.13861 β=102.21°	-37.29272	0.49152	122.534	138.783
CO_2 molecule	P_1		a=20 (fixed)	-22.99409	0.31598		213.388
CO molecule	P_1		a=20 (fixed)	-14.81380	0.13412		197.66
O_2 molecule	P_1		a=20 (fixed)	-8.73325	0.09763		205.15

[a] Obtained from HSC Chemistry Package [52].

Table 2. Calculated thermodynamic properties of CO_2 and CO captured by $NaCoO_2$. T_1 and T_2 are the turnover temperatures of the CO_2 capture reactions at P_{CO2} =0.1 bar for post-combustion, P_{CO2}=20 bar for pre-combustion condition. For NaOH, assuming P_{H2O}=1 bar.

Reactions	**CO_2 or CO** (wt%)	**ΔE^{DFT}** (kJ/mol)	**ΔH** (kJ/mol)	**ΔG** (kJ/mol)	**T_1** (K)	**T_2** (K)
$2NaCoO_2 + CO_2 = Na_2CO_3 + Co_2O_3$	19.31	-121.260	-117.934	-75.432	725	985
$2NaCoO_2 + CO = Na_2CO_3 + 2CoO$	12.29	-115.222	-112.839	-91.954	hT[b]	hT
$2NaCoO_2+CO+{}^1/_2O_2 = Na_2CO_3+Co_2O_3$	12.29	-489.227	-476.121	-407.672	hT	hT

[a] Taken from Ref [43].

[b] hT stands for the temperature out of the range of 1500K

FIGURE 1

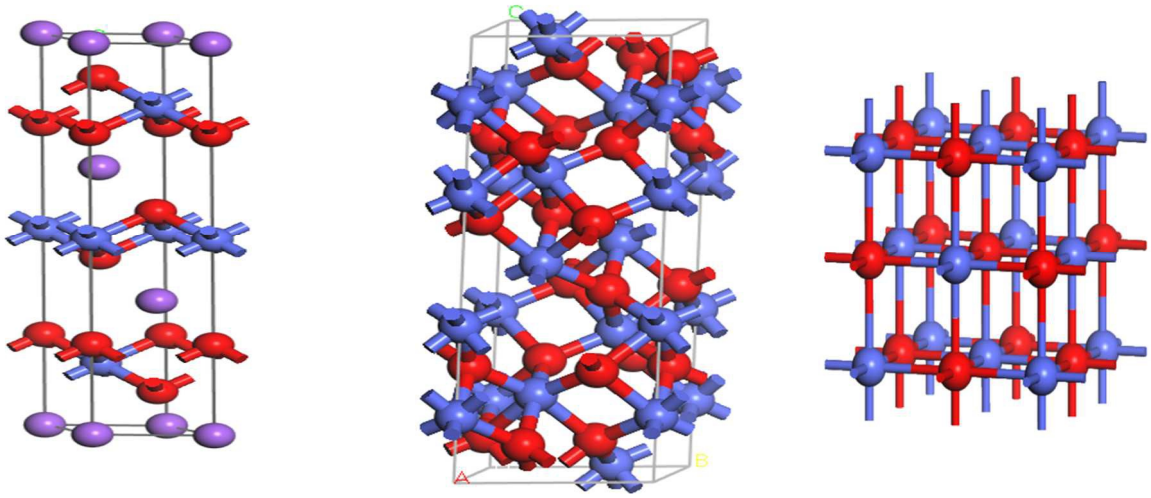

FIGURE 2

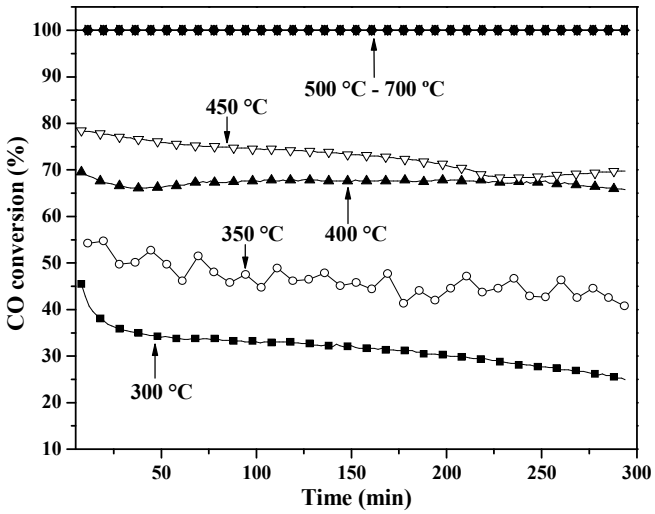

FIGURE 3

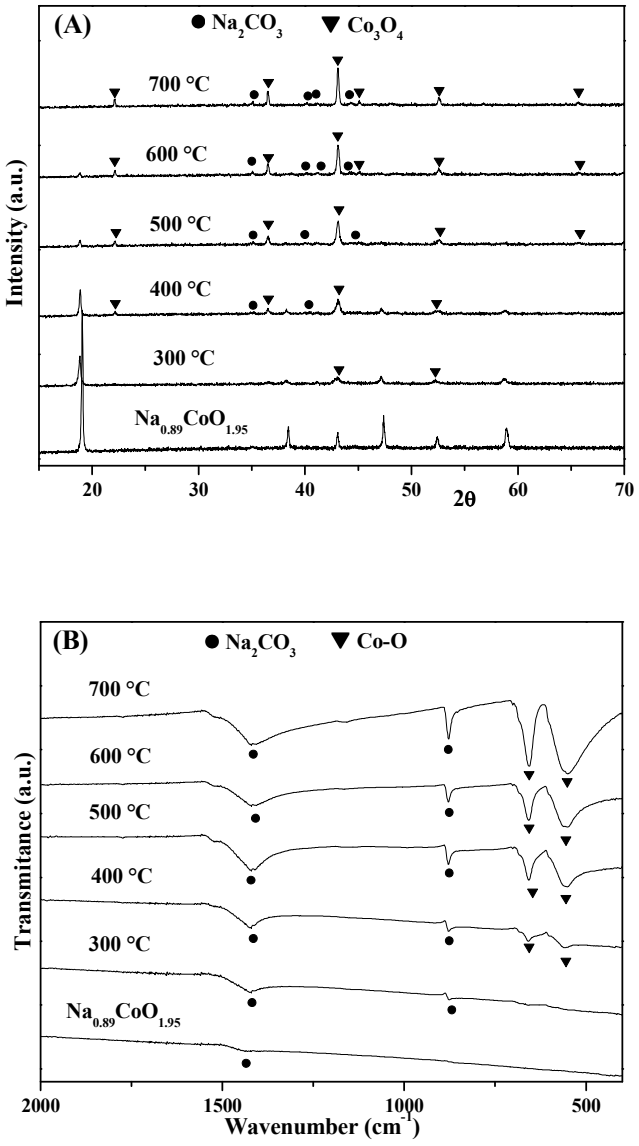

FIGURE 4

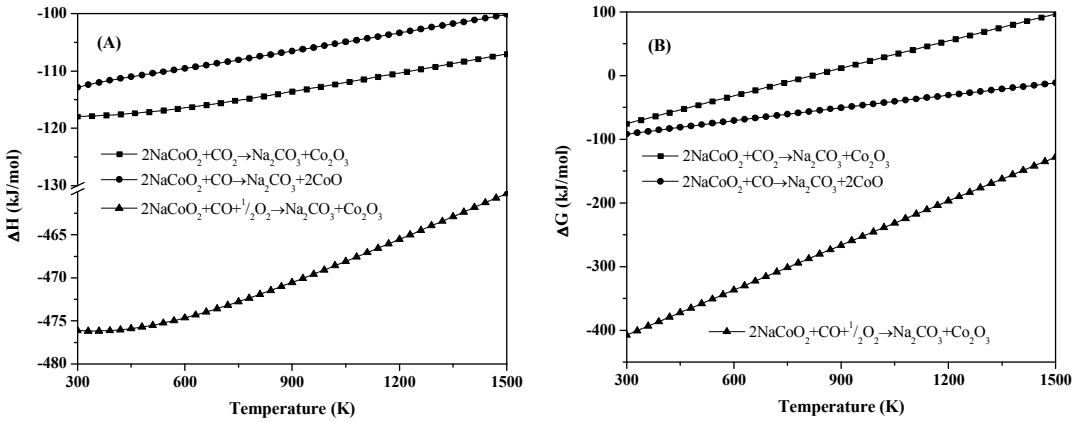

FIGURE 5

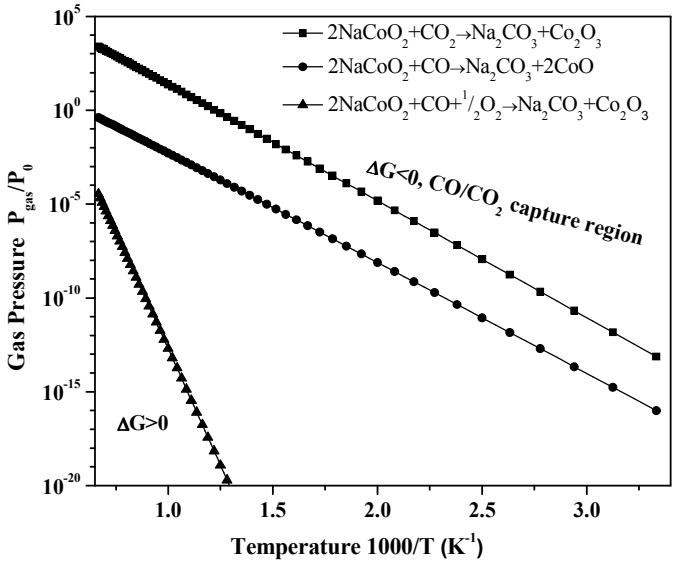

FIGURE 6

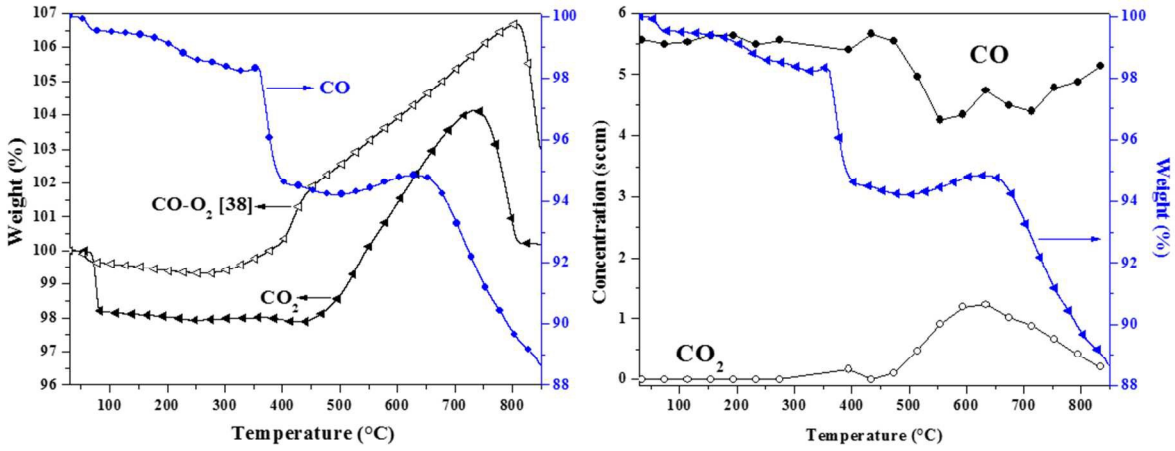

FIGURE 7

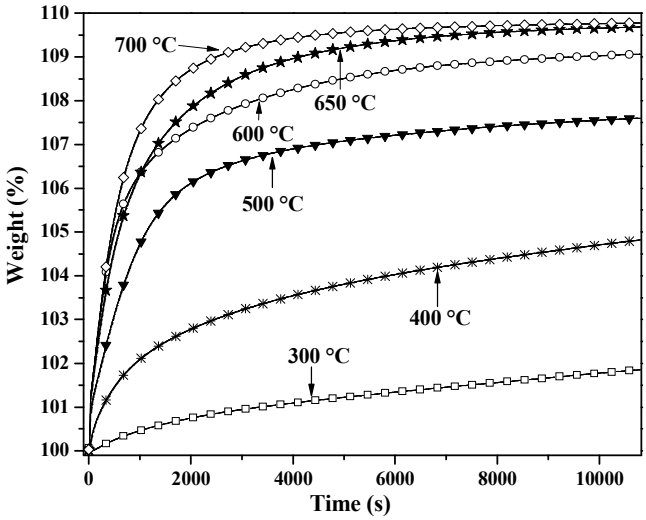

FIGURE 8

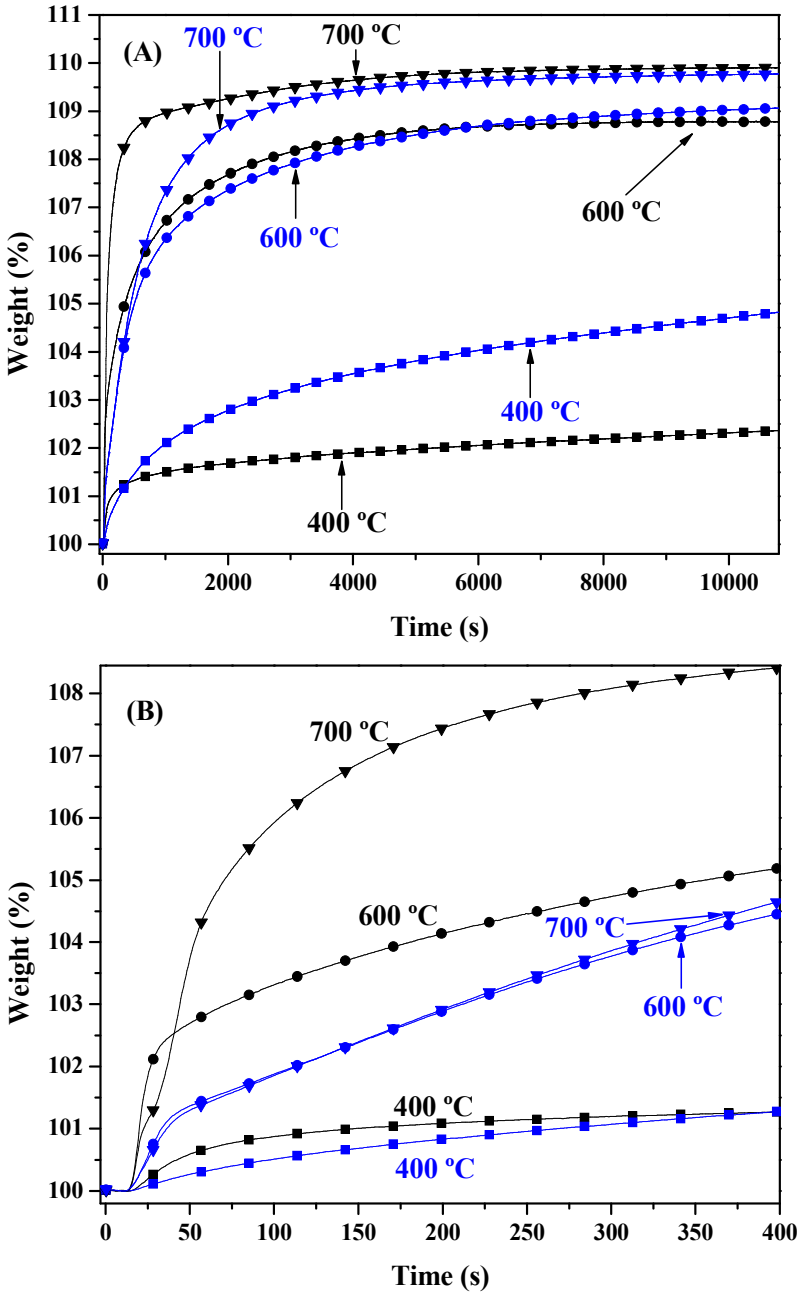

FIGURE 9

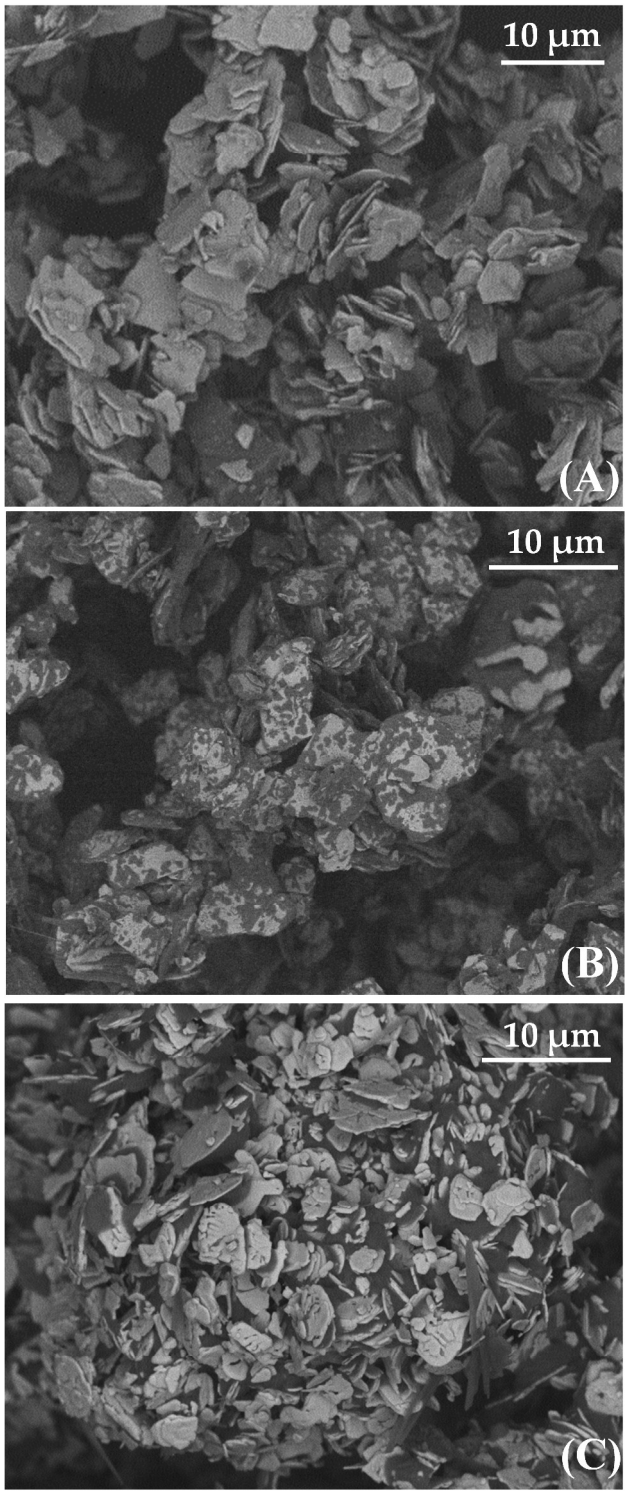

Table of contents

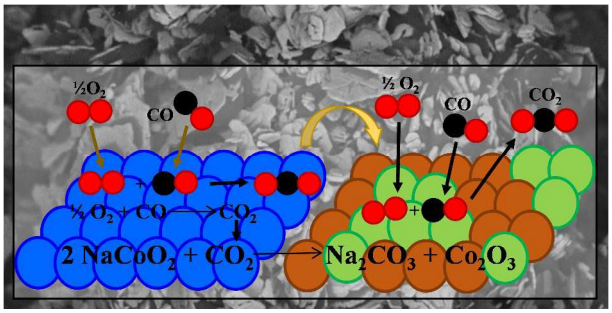

Sodium cobaltate works as a bifunctional material, in the catalysis of CO oxidation and subsequent CO_2 chemisorption.